

Minimal nonlinear dynamical system for the interaction between vorticity waves and shear flows

Erik Gengel^{✉*} and Eyal Heifetz[†]

Department of Geophysics, Porter School of the Environment and Earth Sciences, Tel Aviv University, Tel Aviv 69978, Israel



(Received 24 March 2022; accepted 31 May 2022; published 21 June 2022)

This study is a direct follow-up of the paper by Heifetz and Guha [*Phys. Rev. E* **100**, 043105 (2019)] on a minimal nonlinear dynamical system, describing a prototype of linearized two-dimensional shear instability. In that paper, the authors describe the instability in terms of an action at a distance between two vorticity waves, each of which propagates counter to its local mean flow as well as counter to the other. Here we add to the model the effect of mutual interaction between the waves and the mean flow, where growth of the waves reduces the mean shear and vice versa. This addition yields oscillatory Hamiltonian dynamics, including states of phase slipping and libration with finite-size wave amplitude oscillations. We find that wave–mean-flow dynamics emerging from unstable normal modes in the linearized stage are doomed to librate around the antiphased neutral configuration in which the waves hinder each other’s counterpropagation rate. We discuss as well how the given dynamics relates to familiar models of phase oscillators.

DOI: [10.1103/PhysRevE.105.065109](https://doi.org/10.1103/PhysRevE.105.065109)

I. INTRODUCTION

Recently, Heifetz and Guha [1] explored a dynamical system stemming from a generic minimal model (denoted hereafter as the HG model) for the interaction at a distance between two counterpropagating vorticity waves in shear flows. It generalized the seminal conceptual model of Hoskins *et al.* [2] for counterpropagating Rossby wave instability in geophysical shear flows to a generic dynamics of counterpropagating vorticity waves found in other systems (e.g., [3–9]). The minimal model describes how two remote waves affect each other’s growth and propagation rate counter to their local mean flow, as well as counter to each other. Despite its nonlinear representation, the model results from linearized two-dimensional shear dynamics, where the waves’ amplitudes are assumed to remain small and therefore do not affect the mean flow. In this study, we extend the minimal model to include the finite wave amplitude dynamics, where energy conservation implies that growth of the waves reduces the mean shear and vice versa.

In the linearized stage, modal instability of small amplitudes is obtained when the waves are phase-locked in a way that their counterpropagation rate balances the shear imposed by the mean flow. Therefore, when reaching finite amplitudes, thus consequently reducing the mean shear, the waves’ counterpropagation rate overcomes the mean shear and phases unlock. This leads to a transient dynamics by which the wave-wave interaction affects the waves’ amplitudes and relative phase, as well as the magnitude of the mean shear. The change in the latter affects the waves’ relative phase and consequently the waves’ growth. We find that this extended mechanism gives rise to a Hamiltonian dynamics in which the waves

settle into a libration or perform phase slippings while their amplitudes remain finite, contrasting the linear wave-wave model, in which the wave amplitudes can grow exponentially.

The paper is organized as follows: In Sec. II we extend the minimal model to allow wave–mean-flow interaction in a simple form. In Sec. III we analyze the stability properties of this model and derive criteria for the emergence of libration states. Next, in Sec. IV we discuss similarities of the vorticity wave dynamics in shear flows with other familiar models of phase oscillators. Finally, in Sec. V we discuss our results and suggest some roots for future work.

II. ADDING WAVE–MEAN-FLOW INTERACTION TO THE HG MODEL

A. Summary of the minimal model

The wave interaction equations, implied in the HG model [1,10], read

$$\dot{Q}_1 = \sigma_1 Q_2 \sin \epsilon, \quad \dot{Q}_2 = \sigma_2 Q_1 \sin \epsilon, \quad (1a)$$

$$\dot{\epsilon}_1 = -\hat{\omega}_1 + \sigma_1 \frac{Q_2}{Q_1} \cos \epsilon, \quad \dot{\epsilon}_2 = -\hat{\omega}_2 - \sigma_2 \frac{Q_1}{Q_2} \cos \epsilon. \quad (1b)$$

Here $Q_{1,2}(t)$ and $\epsilon_{1,2}(t)$ are the amplitudes and phases of two counterpropagating vorticity waves $q_{1,2}(t) = Q_{1,2} e^{i\epsilon_{1,2}}$ in regions (1,2) in the (x, y) plane, separated from each other in the y direction, as illustrated in Fig. 1.

Region 1 is governed by a mean flow in the positive x direction, $U_1 > 0$, and region 2 is governed by a negative mean flow, $U_2 < 0$. $\hat{\omega}_{1,2} = k(U_{1,2} + c_{1,2})$ are the waves’ frequencies, in the absence of interaction, viewed from a frame of rest, where $c_{1,2}$ are the intrinsic propagation phase speeds of the waves counter to their local mean flow and counter to each other [$\text{sgn}(c_{1,2}) = -\text{sgn}(U_{1,2})$ and $\text{sgn}(c_1) = -\text{sgn}(c_2)$], where k is their wave number. Generally, $\hat{\omega}_{1,2}$ can take any sign according to the efficiency of the wave

*egiu@gmx.de

†eyalh@tauex.tau.ac.il

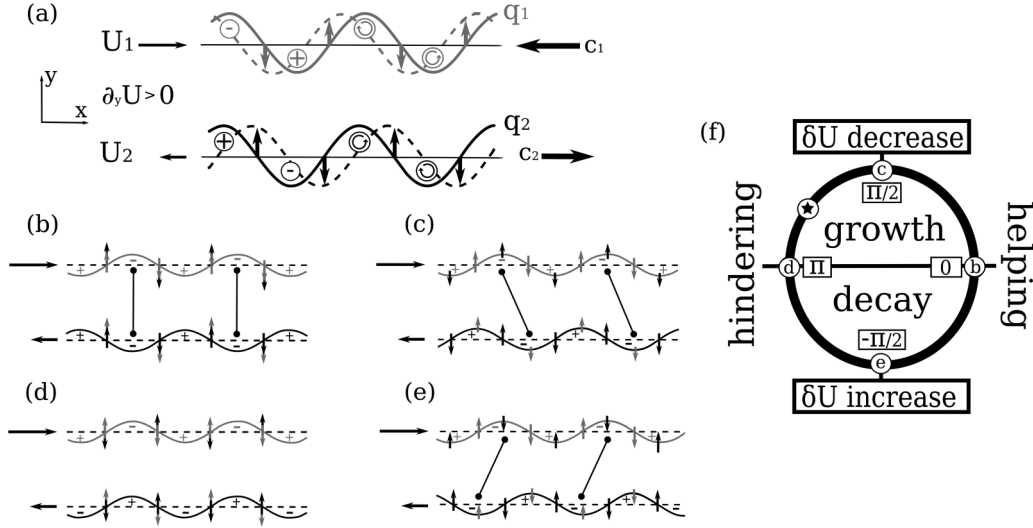


FIG. 1. Schematic overview of the minimal model. (a) Counterpropagation mechanism of the vorticity waves $q_1(t)$ and $q_2(t)$, in regions (1,2), propagating counter to their local mean flows $U_{1,2}$. (b)–(f) Wave interaction at a distance as a function of the vorticity phase difference $\epsilon = \epsilon_1 - \epsilon_2$. The far velocity field induced by one wave on the other may affect the latter’s counterpropagation rate and amplitude: (b) $\epsilon = 0$ —the waves help each other to counterpropagate against the mean flow. (c) $\epsilon = \pi/2$ —the waves amplify each other’s amplitudes (the inclined lines indicate that the total vorticity perturbation is tilted against the action of the shear). (d) $\epsilon = \pi$ —the waves hinder each other’s counterpropagation speed. (e) $\epsilon = 3\pi/2$ —the waves decay each other’s amplitudes (the vorticity perturbation is tilted with the action of the shear). (f) Polar phase diagram of the wave interaction mechanism. Any point on the circle represents different phase configurations (for instance, the star indicates a growing-hindering configuration as $\pi > \epsilon^* < \pi/2$). Since wave growth (decay) leads to decay (growth) of the shear $\delta U_{12} = U_1 - U_2$, the latter decreases (increases) in the upper (lower) part of the circle.

counterpropagation mechanism and the magnitude of the locally opposing mean flow. In Fig. 1(a), the counterpropagation is depicted. Wavy lines represent the wave displacement, and counterclockwise (clockwise) circulations represent positive (negative) vorticity anomalies carried by the waves. In region 1 (2), the wave’s vorticity and displacement are in antiphase (in phase). Consequently, the velocity induced by the vorticity anomalies (indicated by vertical arrows) translates the wave displacement to the left (right) in region 1 (2), as illustrated by the dashed wavy lines, yielding, therefore, negative (positive) intrinsic phase speeds $c_1 < 0$ ($c_2 > 0$).

Equation set (1) describes the interaction of the waves at a distance. This interaction is realized by the evanescent far-field velocity, induced by the localized vorticity anomalies of the waves. The strength of the interaction at a distance is given by positive-definite coupling constants $\sigma_{1,2}$ whose values depend on the specific problem at hand (obtained mathematically by Green’s function described by the vorticity inversion, e.g., [11]). As illustrated in Fig. 1, the velocity field induced by each wave on the other may affect both the propagation rate and the amplitude of the opposed waves. The part of the induced velocity that is in phase (antiphased) with the velocity of the other wave helps (hinders) the latter to propagate counter to its local mean flow. Furthermore, the part of the induced velocity field that is in phase (antiphased) with the displacement of the other wave causes the latter to grow (decay). As will be discussed in Sec. II C, when the waves manage to be phase-locked (that is, to tune their phase speeds to propagate in concert) in a growing configuration, modal insatiability of exponential growth is obtained.

Equation set (1 a) conserves the total wave action:

$$\mathcal{A}_{\text{tot}} = \mathcal{A}_1 + \mathcal{A}_2, \quad (2)$$

where $\mathcal{A}_1 = [Q^2/(2\sigma)]_1$ and $\mathcal{A}_2 = -[Q^2/(2\sigma)]_2$. Furthermore, Eqs. (1 a)–(1 b) conserve the wave pseudoenergy:

$$\begin{aligned} \mathcal{H}_{\text{ww}} &\equiv -(\hat{\omega}_1 \mathcal{A}_1 + \hat{\omega}_2 \mathcal{A}_2) \\ &- 2i\sigma \sqrt{\mathcal{A}_1} \sqrt{\mathcal{A}_2} \cos \epsilon = \mathcal{A}_1 \dot{\epsilon}_1 + \mathcal{A}_2 \dot{\epsilon}_2. \end{aligned} \quad (3)$$

Hereafter, we use the convention that $\sqrt{\mathcal{A}_1} = +[Q/\sqrt{2\sigma}]_1$, $\sqrt{\mathcal{A}_2} = +i[Q/\sqrt{2\sigma}]_2$. The subscript “ww” denotes wave-wave interaction and $\sigma \equiv \sqrt{\sigma_1 \sigma_2}$ is the geometric mean of the interaction coefficients. Heifetz and Guha [1] showed then that equation set (1) obeys a canonical generalized action-angle form, in which \mathcal{H}_{ww} serves as the Hamiltonian:

$$\dot{\mathcal{A}}_1 = -2i\sigma \sqrt{\mathcal{A}_1} \sqrt{\mathcal{A}_2} \sin \epsilon = -\frac{\partial \mathcal{H}_{\text{ww}}}{\partial \epsilon_1}, \quad (4a)$$

$$\dot{\mathcal{A}}_2 = 2i\sigma \sqrt{\mathcal{A}_1} \sqrt{\mathcal{A}_2} \sin \epsilon = -\frac{\partial \mathcal{H}_{\text{ww}}}{\partial \epsilon_2}, \quad (4b)$$

$$\dot{\epsilon}_1 = -\hat{\omega}_1 - i\sigma \frac{\sqrt{\mathcal{A}_2}}{\sqrt{\mathcal{A}_1}} \cos \epsilon = \frac{\partial \mathcal{H}_{\text{ww}}}{\partial \mathcal{A}_1}, \quad (4c)$$

$$\dot{\epsilon}_2 = -\hat{\omega}_2 - i\sigma \frac{\sqrt{\mathcal{A}_1}}{\sqrt{\mathcal{A}_2}} \cos \epsilon = \frac{\partial \mathcal{H}_{\text{ww}}}{\partial \mathcal{A}_2}. \quad (4d)$$

The dynamics following from \mathcal{H}_{ww} is similar to a complex amplitude dynamics in the limit of vanishing dissipation [12,13]. On the contrary, if damping due to viscosity effects is present, then eventually \mathcal{A}_1 and \mathcal{A}_2 approach constant values, and the dynamics reduces to a phase-oscillator model of the Kuramoto-type [9,14].

B. Wave-mean flow interaction

As a consequence of energy conservation, the growth of wave amplitudes to a finite level must come at the expense of the mean flow energy, leading to a variation $\delta U_{1,2}(y, t) \equiv U_1 - U_2$ of the mean flow. For vortical wave-mean flow interaction, $\dot{U}(y, t) = -\dot{A}(y, t)$, e.g., [15]. Since our model is crude and contains only two bulks of the mean flow (rather than a continuous profile), we represent the averaging effect of the wave action growth on the bulk mean flow velocities by two nondimensional positive-definite constants, $\alpha_{1,2}$, whose values depend on the details of the problem, so that $\dot{U}_{1,2} = -[\alpha \dot{A}]_{1,2}$. As $\text{sgn}(A_i) = \text{sgn}(U_i)$, growth in the wave vorticity amplitudes decreases the absolute value of the mean flow in their region and thus the kinetic energy of the mean flow. From Eqs. 1(a), (4a), and (4b) and Fig. 1, it is clear that this scenario happens when the vorticity field of wave 1 lags behind wave 2 ($0 < \epsilon < \pi$), e.g., Fig. 1(c). Since $\partial_y U(y) > 0$, this situation can be envisioned by a vorticity field tilted against the mean shear. Vice versa, when the vorticity field is tilted with the mean shear ($-\pi < \epsilon < 0$), e.g., Fig. 1(e), the wave energy is deposited back into the mean flow.

Hereafter, we assume that this is the only consequence of the wave-mean flow interaction, although generally (according to the details of the problem at hand) it may alter the interaction coefficients $\sigma_{1,2}$, as well as the intrinsic counterpropagation phase speeds of the waves, $c_{1,2}$, with respect to the mean flow. Furthermore, in order to focus on the wave-mean-flow interaction, we ignore resonant triad interactions affecting the dynamics (e.g., [16]). Hence, our only modification to the minimal model is by allowing the frequencies to vary with time:

$$\hat{\omega}_{1,2} = -[\beta \dot{A}]_{1,2}, \quad (5)$$

with $\beta_{1,2} \equiv k\alpha_{1,2}$, so that $[\partial \hat{\omega} / \partial \mathcal{A}]_{1,2} = -\beta_{1,2}$. Quite remarkably, this modification conserves the canonical Hamiltonian structure of (4), with the same total wave-action constant of motion, \mathcal{A}_{tot} , but with a modified Hamiltonian constant of motion \mathcal{H}_{wwm} ,

$$\mathcal{H}_{\text{wwm}} = \mathcal{H}_{\text{ww}} + \mathcal{H}_{\text{wm}}, \quad \mathcal{H}_{\text{wm}} \equiv -\frac{1}{2}(\beta_1 \mathcal{A}_1^2 + \beta_2 \mathcal{A}_2^2), \quad (6)$$

that is replacing \mathcal{H}_{ww} on the right-hand side of (4) (where the subscripts “ww” and “wm” stand, respectively, for the combined wave-wave-mean-flow and the wave-mean-flow interactions).

C. Antisymmetric wave-action dynamics

The essence of the nonlinear wave-wave-mean-flow interaction can be understood for vanishing total action $\mathcal{A}_{\text{tot}} = 0$. In that case, $\mathcal{A}_1 = -\mathcal{A}_2 \equiv \mathcal{A} \equiv Q^2/2\sigma$, thus the wave-action is antisymmetric. Equation set (4) then simplifies to

$$\frac{d\epsilon}{d\tau} = 2 \cos \epsilon - \mu, \quad \frac{d\mathcal{A}}{d\tau} = 2\mathcal{A} \sin \epsilon. \quad (7)$$

Here, time is scaled by the mean interaction coefficient, $\tau \equiv \sigma t$, and $\mu \equiv \hat{\omega}/\sigma$ is the control parameter of the linearized dynamics, representing the ratio between the tendency of the waves to propagate in opposite directions ($\hat{\omega} \equiv \hat{\omega}_1 - \hat{\omega}_2$)

and the wave interaction (given by the mean interaction coefficient σ), acting to “tie” them together.

Antisymmetric wave-action dynamics is of special importance. In the minimal model, the phase evolution (7) is independent of the waves’ amplitude. Moreover, it allows a resonance mechanism leading to exponential growth of the waves’ amplitudes. This occurs when the waves are phase-locked ($d\epsilon/d\tau = 0$) in a growing configuration ($\pi > \epsilon > 0$) to maintain mutual amplification, Fig. 1(f). The resonance mechanism is the wave interaction interpretation for the modal instability in the linear stage. Phase-locking is obtained if $\cos \epsilon_0 = \mu/2$ and therefore it sets a range $-2 \leq \mu \leq 2$. The scaled exponential growth rate, $2 \sin \epsilon_0$, obtained from (7), is then positive for the growing normal modes ($\pi > \epsilon_0 > 0$) and negative for the decaying ones ($-\pi < \epsilon_0 < 0$).

The dynamics of system (7) is demonstrated in Figs. 2(a)–2(f) in the plane $(X, Y) = \mathcal{A}(\cos \epsilon, \sin \epsilon)$ for different values of the control parameter μ . The phase plane flow in polar coordinates then reads

$$U_\epsilon \equiv \mathcal{A} \frac{d\epsilon}{d\tau} = 2X - \mu\mathcal{A}, \quad U_{\mathcal{A}} \equiv \frac{d\mathcal{A}}{d\tau} = 2Y. \quad (8)$$

For $|\mu| > 2$ [Figs. 2(a) and 2(f)], the phase portrait is composed of elliptic trajectories whose semimajor axis lays on the X axis. As no modal exponential growth is permitted, the amplitude is bounded and varies along the periodic orbits [as demonstrated in Figs. 2(g) and 2(h) for $\mu = -2.5$]. For $|\mu| < 2$ [Figs. 2(b)–2(e)], the phase converges rapidly to the unstable modal phase ϵ_0 [e.g., the sigmoidlike structure in Fig. 2(i), corresponding to the dynamics in Fig. 2(c), for $\mu = -1.5$] and all amplitudes, after a short transient stage, grow practically exponentially, Fig. 2(j) (unless initiated at the exact decaying modal configuration of $\epsilon = -\epsilon_0$).

We assume that wave-mean-flow interaction becomes relevant when the waves reach the finite wave-action amplitude that is larger by, say, two orders of magnitude than its initial one (that is, by one order of magnitude for the vorticity amplitude Q). We see that such finite amplitudes are reached when $|\mu| < 2$, as then the waves converge rapidly into the growing mode configuration with phase difference ϵ_0 . This phase corresponds to a counterpropagation speed that balances the mean shear such that $\mu_0 = 2 \cos \epsilon_0$. Additionally, values of $|\mu|$ only slightly above 2 can give rise to a bottleneck in the phase dynamics such that the system spends an exceedingly long time in a growing configuration. In those cases, the waves may temporarily reach finite amplitudes as well. Consequently, we assume that the initial conditions for the wave-mean-flow interaction model are when the waves possess (i) finite amplitude \mathcal{A}_0 and (ii) relative phase difference ϵ_0 .

D. Wave-wave-mean-flow interaction model for antisymmetric wave-action dynamics

As the waves’ amplitudes grow, the mean shear decays. According to (5),

$$\frac{d\mu}{d\tau} = -2 \frac{\bar{\beta}}{\sigma} \frac{d\mathcal{A}}{d\tau}, \quad (9)$$

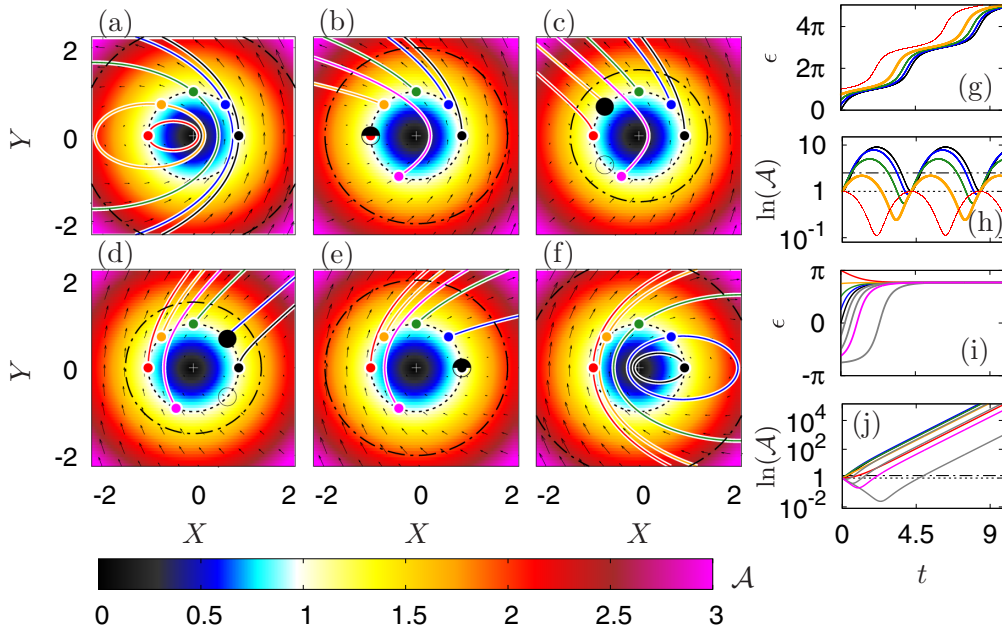


FIG. 2. (a)–(f) Phase plane portrait of the antisymmetric wave-action dynamics, described by Eq. (7), with $X = \mathcal{A} \cos \epsilon$ and $Y = \mathcal{A} \sin \epsilon$. Shown are the unit circle $\mathcal{A} = 1$ (dashed) and the circle at which $\mathcal{A} = |\mu_0|$ (dotted-dashed). Trajectories starting at angles $\epsilon \in [0, \pi/4, \pi/2, 3\pi/4, \pi, 11\pi/8]$ are shown in black, blue, green, orange, red, and magenta, respectively. (a) $\mu = -2.5$, (b) $\mu = -2$, (c) $\mu = -1.5$, (d) $\mu = 1.5$, (e) $\mu = 2$, and (f) $\mu = 2.5$. The large black dots in (b)–(e) indicate the phase difference ϵ_0 , in the unstable mode configuration (filled markers), and the decaying ones $-\epsilon_0$ (empty markers). Also, shown as a color map is the amplitude \mathcal{A} . Panels (g),(h) show phase slips of $\epsilon(t)$ and oscillations of $\ln(\mathcal{A})(t)$ for trajectories shown in panel (a). Panels (i),(j) are similar but show phase locking and amplitude growth corresponding to panel (c). Additional initial phases (gray) $\epsilon \in [5\pi/4, 3\pi/2, 7\pi/4]$ first decrease in amplitude before they grow.

where $\bar{\beta} \equiv (\beta_1 + \beta_2)/2$ is the mean-wave–mean-flow interaction coefficient. Consequently, the immediate effect of the wave–mean-flow interaction is that $\mu(t)$ becomes smaller than μ_0 and the phase difference ϵ becomes larger than ϵ_0 , as now the waves’ counterpropagation rate overcomes the mean shear and the phase unlocks. This tendency is expected to go on until $\epsilon(t) > \pi$, as then the wave-wave interaction reduces each other’s amplitude and consequently the mean shear regains strength and acts to shift the waves back to a growing configuration.

The transient dynamics can therefore be formulated as follows. We first rescale the wave action: $\tilde{\mathcal{A}} \equiv 2\frac{\bar{\beta}}{\sigma}\mathcal{A}$, so that the wave–mean-flow interaction of (9) implies

$$\frac{d\mu}{d\tau} = -\frac{d\tilde{\mathcal{A}}}{d\tau} \implies \tilde{\mathcal{A}}(t) + \mu(t) = \tilde{\mathcal{A}}_0 + \mu_0 \equiv \gamma_0. \quad (10)$$

Implementing (7) with the wave-wave interaction dynamics, we obtain the two equivalent forms of the modified model, in terms of the variable pairs (ϵ, μ) or $(\epsilon, \tilde{\mathcal{A}})$:

$$\frac{d\epsilon}{d\tau} = 2 \cos \epsilon - \mu, \quad \frac{d\mu}{d\tau} = 2(\mu - \gamma_0) \sin \epsilon, \quad (11)$$

$$\frac{d\epsilon}{d\tau} = 2 \cos \epsilon + \tilde{\mathcal{A}} - \gamma_0, \quad \frac{d\tilde{\mathcal{A}}}{d\tau} = 2\tilde{\mathcal{A}} \sin \epsilon, \quad (12)$$

with γ_0 as a control parameter. Exemplary solutions of Eqs. (11) and (12) are depicted in Figs. 3 and 4.

It is straightforward to verify then that systems (11) and (12) conserve the respective constant of motion:

$$\mathcal{E} = \mu^2 + 4(\gamma_0 - \mu) \cos \epsilon = \tilde{\mathcal{A}}^2 + 2\tilde{\mathcal{A}}(2 \cos \epsilon - \gamma_0) + \gamma_0^2, \quad (13)$$

which is related to the Hamiltonian \mathcal{H}_{wvm} , under the constraint $\mathcal{A}_{\text{tot}} = 0$. Using (3), (6), and (13), we obtain that indeed

$$\begin{aligned} \mathcal{H}_{\text{wvm}}^{(\mathcal{A}_{\text{tot}}=0)} &= (2\sigma \cos \epsilon - \hat{\omega})\mathcal{A} - \bar{\beta}\mathcal{A}^2 \\ &= \frac{\sigma^2(\mathcal{E} - \gamma_0^2)}{4\bar{\beta}} = -\bar{\beta}\mathcal{A}_0^2. \end{aligned} \quad (14)$$

III. ANALYSIS OF THE EXTENDED MODEL

A. Stability of fixed points

The fixed points of (11) and (12) are

$$\begin{aligned} (\epsilon, \mu, \tilde{\mathcal{A}})^* &= [(0, 2, \gamma_0 - 2); (\pi, -2, \gamma_0 + 2); \\ &(\pm \cos^{-1}(\gamma_0/2), \gamma_0, 0)]. \end{aligned} \quad (15)$$

The first two correspond to the cases in which the waves are either in phase or antiphased. These fixed points can be regarded as a limiting case of the fixed points of (7) in the linearized dynamics, as for these configurations the waves’ amplitude growth is zero and consequently the mean shear remains unchanged. The major difference between the linearized and the nonlinear model is their stability properties.

In the linearized model, the two points are semistable as a small perturbation $\delta\epsilon$ evolves according to the second-order

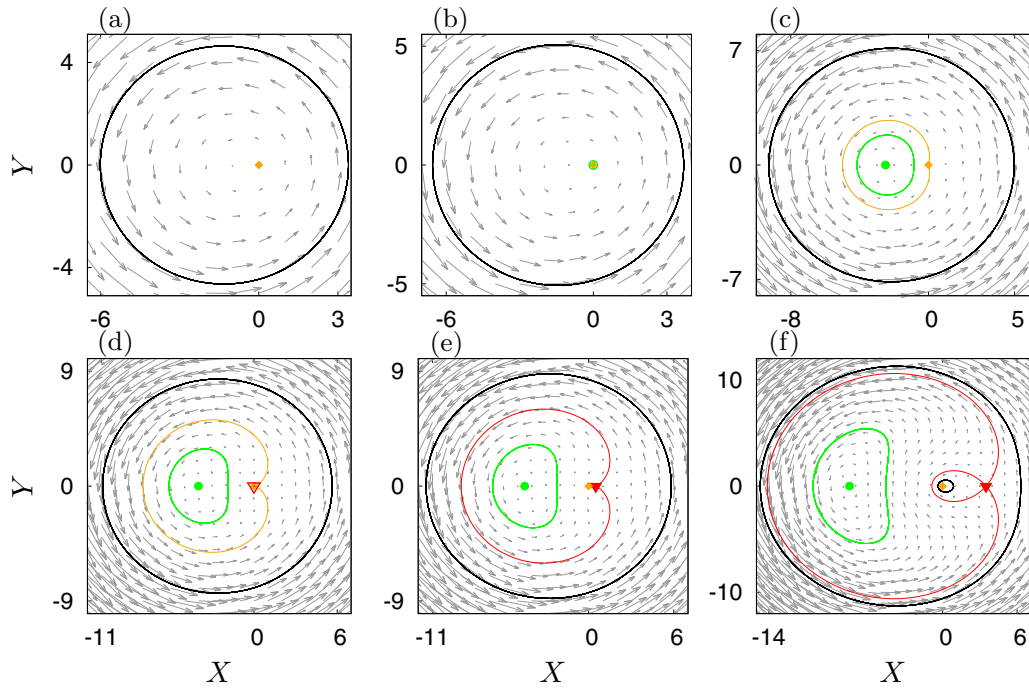


FIG. 3. Depicted are the polar vector fields corresponding to Eq. (12) (gray arrows), the fixed points, and the homoclinic orbits for different γ_0 . $X = \tilde{A} \cos(\epsilon)$ and $Y = \tilde{A} \sin(\epsilon)$. (a) $\gamma_0 = -2.5$, (b) $\gamma_0 = -2.0$, (c) $\gamma_0 = 0.5$, (d) $\gamma_0 = 2.0$, (e) $\gamma_0 = 2.5$, and (f) $\gamma_0 = 5.5$. Shown as red triangles is the saddle point at $(\epsilon^*, \mu^*) = (0, 2)$. Shown as a green dot is $(\epsilon^*, \mu^*) = (\pi, -2)$. Orange diamonds indicate $(\epsilon^*, \mu^*) = (\pm \arccos(\gamma_0/2), \gamma_0)$. Orange and red curves show the polar homoclines corresponding to Eqs. (18) and (19). The green circular line indicates a libration solution of Eq. (12). Black circular lines represent trajectories of free rotation (phase slips). The panels correspond to energies shown in Fig. 4.

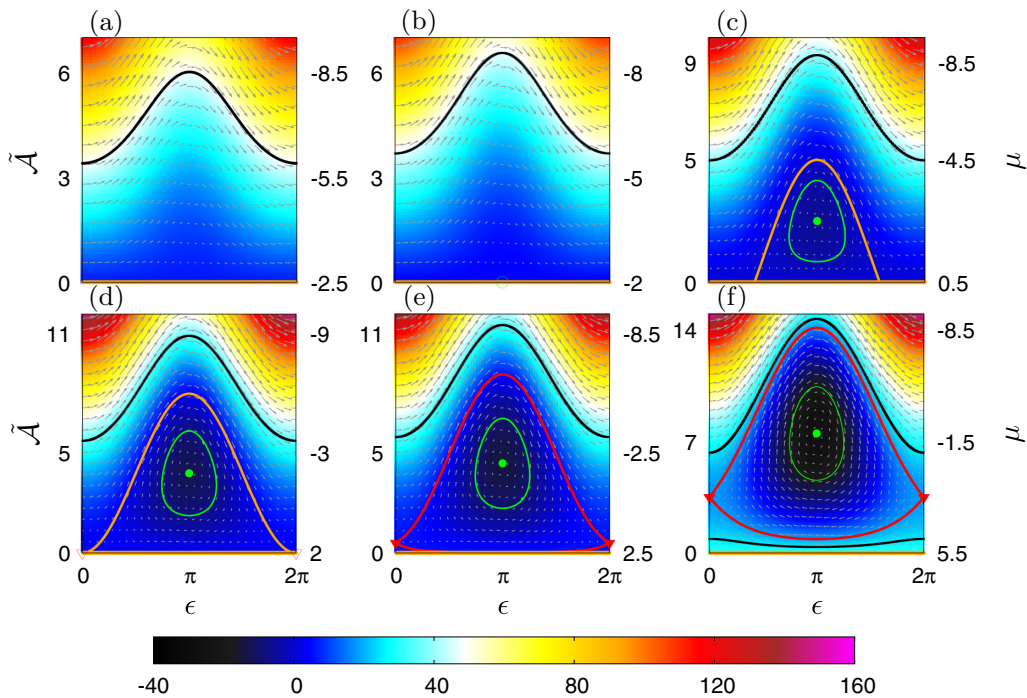


FIG. 4. Depicted are energy surfaces $\mathcal{E}(\tilde{A}, \epsilon)$ (color map) corresponding to Fig. 3. The right-hand scale represents the frequencies μ . Orange and red lines show the homoclines associated with the fixed point at $\tilde{A}^* = 0$ and $\epsilon^* = 0$, respectively. The green circular line indicates a libration solution of Eqs. (11) and (12). The top black lines [as well as the bottom black line in panel (f)] are trajectories of free rotation (phase slips).

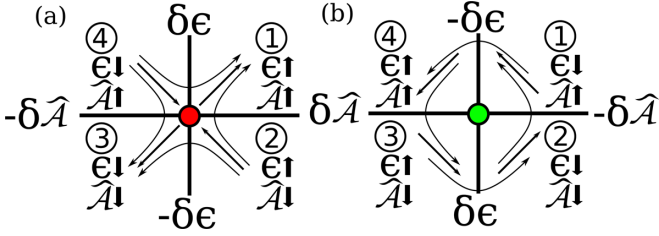


FIG. 5. Schematic illustration of the in-phase fixed point (a) and the antiphase fixed point (b). Tendencies of amplitude perturbations $\delta\tilde{A}$ and phase perturbations $\delta\epsilon$ are indicated in the four quadrants surrounding the fixed points.

dynamics:

$$\frac{d}{d\tau}\delta\epsilon = -(\delta\epsilon)^2 \text{ at } \epsilon^* = 0 \quad \text{and} \quad \frac{d}{d\tau}\delta\epsilon = (\delta\epsilon)^2 \text{ at } \epsilon^* = \pi. \quad (16)$$

For the in-phase state, this means that a slight increase or decrease of the phase difference reduces the ability of the waves to help each other to counterpropagate, thus the (unaffected) mean shear prevails and acts to decrease the phase between the waves. By the same logic, when the waves are stationary in a fully hindering configuration ($\epsilon^* = \pi$), a slight change in their phase allows the counterpropagation rate to overcome the mean shear, and the phase between the waves increases.

In the nonlinear model, the Jacobian of either (11) or (12) yields the eigenvalues $\lambda_{1,2} = \pm\sqrt{2(\gamma_0 - \mu^*)} = \pm\sqrt{2\tilde{A}^*}$ for the fixed point at $\epsilon^* = 0$, thus for the physically relevant case of $\tilde{A}^* > 0$ the point becomes a saddle node [Fig. 5(a)]. For the fixed point at $\epsilon^* = \pi$, $\lambda_{1,2} = \pm i\sqrt{2(\gamma_0 - \mu^*)} = \pm i\sqrt{2\tilde{A}^*}$, hence the point becomes a center [Fig. 5(b)]. The perturbation first-order dynamics at these fixed points are

$$\frac{d}{d\tau}\delta\epsilon = \delta\tilde{A} = -\delta\mu, \quad \frac{d}{d\tau}\delta\tilde{A} = -\frac{d}{d\tau}\delta\mu = \pm 2\tilde{A}^*\delta\epsilon, \quad (17)$$

where the plus (minus) sign in the second equation of Eqs. (17) corresponds to $\epsilon^* = 0$ ($\epsilon^* = \pi$). The reason why the in-phase fixed point becomes a saddle results from the fact that an increase in the phase difference brings the system into the growing waves' amplitude configuration [Fig. 5(a), regions 1,4]. Consequently near $\epsilon^* = 0$, when the phase difference grows, this leads to growth of the waves' amplitudes and thus a reduction of the mean shear, which allows further growth of the phase difference, and so on. In contrast, the out-of-phase fixed point becomes a center, as an increase in the phase transfers the waves into the decaying configuration [Fig. 5(b), regions 1,4]. As the waves' amplitudes decays, the shear is recovered and pushes the waves back. When the phase crosses the fixed point and becomes smaller than π [Fig. 5(b), regions 2,3], the waves' amplitudes grow, the shear is reduced, and thus the phase is pushed back from the other side toward the fixed point. This yields harmonic oscillations with a frequency of $\sqrt{2\tilde{A}^*}$.

The additional pair of fixed points in (15) with the vanishing wave amplitudes ($\tilde{A}^* = 0$) possess the eigenvalues, $\lambda_{1,2} = \pm 2\sin\epsilon^*$. They correspond to the linearized dynamics of the emergence of small wave amplitudes, where instability

(stability) is obtained when the waves are “born” in the growing (decaying) configuration.

B. Homoclinic orbits

In Figs. 3 and 4, we show the phase plane flows in the coordinates $(X, Y) = (\tilde{A}(\cos\epsilon, \sin\epsilon))$ and $(X, Y) = (\epsilon, \tilde{A})$, respectively, for various values of the control parameter γ_0 . For $\gamma_0 < -2$, no fixed points exist, the flow is rotational, and ϵ increases monotonically (wave motion against the shear). When $\gamma_0 > -2$, the fixed points at $\epsilon^* = \pi$ and at $\tilde{A}^* = 0$ emerge. Then the main branch of the homocline (indicated by the orange curves in Figs. 3 and 4),

$$\begin{aligned} \tilde{A}_{\text{homoc}} &= 2(\gamma_0 - 2\cos\epsilon), \\ \mu_{\text{homoc}} &= 2\cos\epsilon \pm |2\cos\epsilon - \gamma_0|, \end{aligned} \quad (18)$$

associated with the fixed point at $\tilde{A}^* = 0$, separates between the inside librated motion around the center $\epsilon^* = \pi$, and the rotational motion outside of it.

When $\gamma_0 > 2$, the saddle node at $\epsilon^* = 0$ is born out of the fixed point of $\tilde{A}^* = 0$, and the dynamics resembles an upside-down nonlinear pendulum, as the center is at $\epsilon^* = \pi$ and the saddle is at $\epsilon^* = 0$. Using the energy conservation of (13), the separatrix homocline (indicated by the red curves in Figs. 3 and 4) attached to the saddle node is found to satisfy the quadratic equations:

$$0 = \tilde{A}_{\text{homoc}}^2 + 2(2\cos\epsilon - \gamma_0)\tilde{A}_{\text{homoc}} + (\gamma_0 - 2)^2, \quad (19a)$$

$$0 = \left(\frac{\mu_{\text{homoc}}}{2}\right)^2 - 2\cos\epsilon\left(\frac{\mu_{\text{homoc}}}{2}\right) + \gamma_0(\cos\epsilon - 1) + 1. \quad (19b)$$

C. Libration or rotation?

As is evident from Figs. 3 and 4, the dynamical system of (11) and (12) allows both librational and rotational motions. This, however, does not guarantee that waves which are emanating from the unstable normal mode (of the phase-locking configuration $\mu_0 = 2\cos\epsilon_0$, where $\pi > \epsilon_0 > 0$) will experience both types of motion. In fact, we now show that regardless of the magnitude of the initial finite amplitude \tilde{A}_0 , all these waves are doomed to librate around the center point of $\epsilon^* = \pi$.

As for these initial conditions $\tilde{A}_0 = \gamma_0 - 2\cos\epsilon_0$, γ_0 must be larger than -2 to allow the onset of positive waves' amplitude. Thus, panels (a),(b) in Figs. 3 and 4 are irrelevant to such dynamics. For the range $-2 < \gamma_0 < 2$ [e.g., panels (c),(d)], rotation is allowed when the value of \tilde{A}_0 is larger than the value of \tilde{A}_{homoc} of homocline (18), at $\epsilon = \epsilon_0$. Plugging \tilde{A}_0 in the homocline equation and using Eq. (10), we immediately obtain, however, that $\tilde{A}_0 = \frac{1}{2}\tilde{A}_{\text{homoc}}$ at $\epsilon = \epsilon_0$, hence only libration is possible. Similarly, in order to obtain rotation for the range $\gamma_0 > 2$ [e.g., panels (e),(f)], \tilde{A}_0 must be either larger than the positive root of \tilde{A}_{homoc} in (19) at $\epsilon = \epsilon_0$, or smaller than its negative root there. Plugging \tilde{A}_0 in (19) for $\epsilon = \epsilon_0$, we obtain the two roots $\tilde{A}_{\text{homoc}} = \tilde{A}_0 \pm \sqrt{\tilde{A}_0^2 - (\gamma_0 - 2)^2}$, from which it is clear that, here as well, the only possible dynamics is libration.

Starting then from the initial unstable modal phase ϵ_0 , with an initial finite amplitude \tilde{A}_0 , the librated dynamics reaches

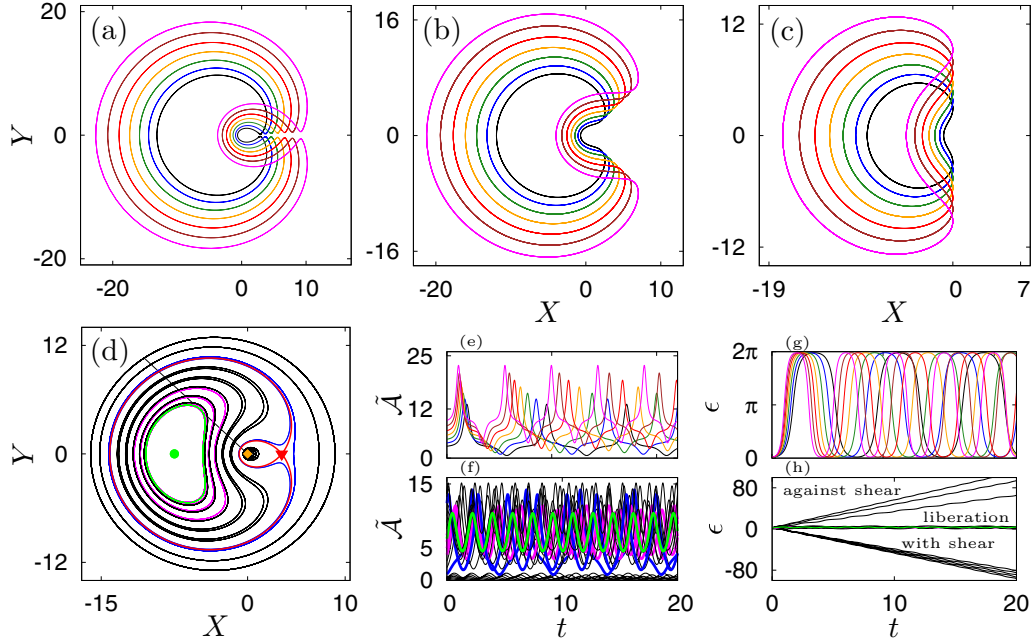


FIG. 6. Depicted are exemplary polar trajectories of the nonlinear system Eq. (12) where $X = \tilde{A} \cos(\epsilon)$ and $Y = \tilde{A} \sin(\epsilon)$ and $\mathcal{A}(t), \epsilon(t)$. Panels (a)–(c) show results for $\tilde{A}_0 \in [2.9, 3.7, 4.6, 5.6, 6.7, 7.9, 9.2]$ in black, blue, green, orange, red, brown, and magenta. These trajectories depart from the initial normal mode conditions $2 \cos \epsilon_0 = \mu_0$. (a) $\epsilon_0 = \pi/50$, $\mu_0 = 1.996$; (b) $\epsilon_0 = \pi/4$, $\mu_0 = 1.414$; (c), $\epsilon_0 = \pi/2$, $\mu_0 = 0$. Panel (d) depicts polar trajectories for $\gamma_0 = 5.5$ all starting at $\epsilon_0 = 3\pi/4$ (black diagonal) and onset amplitudes of $\tilde{A} \in [0.1, 0.2, 0.3, 0.4, 0.5, 1, 2, \dots, 15]$. Shown in red are the homocline of (19) and the in-phase saddle point. The origin and the antiphase fixed point are indicated, respectively, by orange and green. The green trajectory is associated with the normal mode initial condition as shown in Fig. 4, panel (f). Magenta trajectories indicate librated solutions for which $|\mu_0| < 2$, and black and blue curves correspond to either libration or rotational trajectories where $|\mu_0| > 2$. Panels (e),(g) Amplitudes $\tilde{A}(t)$ and $\epsilon(t)$ for panel (a). (f),(h) Amplitudes and phases for panel (d).

its maximum amplitude after a period of amplitude growth at $\epsilon = \pi$ (as indicated from Fig. 4). When the waves cross this point, the wave interaction begins to reduce the waves' amplitudes. Equating the energy expression in (13) between

the initial modal position $(\tilde{A}_0, \epsilon_0)$ and the maximum amplitude position (\tilde{A}_{\max}, π) , we obtain that the maximal additional growth, resulting from the wave–mean-flow interaction, is given by

$$\tilde{A}_{\max} - \tilde{A}_0 = 2 \cos \epsilon_0 + 2 \sqrt{\cos \epsilon_0 (\cos \epsilon_0 + \tilde{A}_0)} = 2 \cos \epsilon_0 + 2 \sqrt{\cos \epsilon_0 (\gamma_0 - \cos \epsilon_0)}, \quad (20)$$

which maximizes when ϵ_0 tends to zero as then the residence time in the growing regime ($\epsilon_0 < \epsilon < \pi$) increases. Panels (a)–(c), in Fig. 6, show various trajectories of libration in the polar plane, starting from the initial unstable modal phases, where panels (e) and (g) show the amplitude and phase evolution from the small initial condition $\epsilon_0 = 0.02\pi$, corresponding to the trajectories in panel (a).

In principle, rotational dynamics can be obtained for imposed finite amplitudes (i.e., when the initial onset does not depart from the growing mode configuration, so that $\mu_0 \neq 2 \cos \epsilon_0$). Using the homocline equations of (18) and (19), we obtain the critical conditions

$$\tilde{A}_0^c = \begin{cases} 2(2 \cos \epsilon_0 - \mu_0) & \text{if } -2 < \gamma_0 < 2, \\ \frac{(2 - \mu_0)^2}{4(1 - \cos \epsilon_0)} & \text{if } \gamma_0 > 2, \end{cases} \quad \text{rotation: } \tilde{A}_0 < \tilde{A}_0^c, \quad \text{libration: } \tilde{A}_0 > \tilde{A}_0^c \quad (21)$$

(where for $\mu_0 = 2 \cos \epsilon_0$, $\tilde{A}_0^c = 0$ if $-2 < \gamma_0 < 2$ and $\tilde{A}_0^c = [\tilde{A}_0 - (\gamma_0 - 2)]/2$ if $\gamma_0 > 2$, thus libration is indeed the only option for positive initial amplitudes). Panel (d) of Fig. 6 is the same as panel (f) of Fig. 3, but it shows more trajectories for the case in which $\gamma_0 = 5.5$. All trajectories start from the phase $\epsilon_0 = 3\pi/4$. The green trajectory corresponds to the libration initiated from the unstable normal mode ($\mu_0 = 2 \cos \epsilon_0 \approx -1.41$, $\tilde{A}_0 = \gamma_0 - \mu_0 \approx 6.91$). The magenta trajectories represent librated solutions for which $|\mu_0| < 2$

[that in the linearized dynamics of HG would have otherwise converge to the unstable mode phase, e.g., panels (b)–(e) of Fig. 2]. Solutions that are colored black are of $|\mu_0| > 2$ [therefore, rotational in the linearized dynamics, e.g., panels (a),(f) of Fig. 2]. They can either librate or rotate in the nonlinear system. For example, for $\mu_0 = 4.5$, $\tilde{A}_0 = 1 > \tilde{A}_0^c \approx 0.91$ [blue trajectory inside the homoclinic basin of panel (d) of Fig. 6], thus libration is obtained. On the contrary, for large enough counterpropagation rate

against the shear, $\mu_0 = -7.5$, $\tilde{A}_0 = 13 < \tilde{A}_0^c \approx 13.22$ and the counterclockwise rotation is maintained in the nonlinear system [blue rotating solution, panel (d) of Fig. 6]. [These trajectories correspond to the free solutions in the upper part of panel (f) of Fig. 4.] For large enough values of μ_0 (strong enough positive shear and relative weak counterpropagation rate) the solutions can be of clockwise rotation and correspond to the dynamics inside the inner loop of the homocline, circulating the origin in panel (d) of Fig. 6. These solutions correspond to the lower part of panel (f) of Fig. 4. For instance, for $\mu_0 = 5$, $\tilde{A}_0 = 0.5 < \tilde{A}_0^c \approx 3.66$. In panels (f),(h) of Fig. 6 we show the corresponding phase and amplitude evolution for these trajectories. We see that large amplitudes correspond to counterclockwise rotation trajectories, medium range for libration, and small amplitudes for clockwise rotational motion.

To summarize, small perturbations that grow by normal mode instability, in the linearized dynamics, will librate around the center point at $\epsilon^* = \pi$, due to the restoring wave mean flow interaction. Other finite amplitude initial condition states will rotate against the mean shear (counterclockwise) if the initial mean shear is weak enough to allow the self counterpropagation rate to keep dominating the dynamics, even when their amplitudes decrease by the wave–mean–flow interaction. This requires relatively large initial waves’ amplitudes. The dynamics can also be clockwise rotation, with the shear, in the opposite case where the initial shear is strong enough to dominate the dynamics, even when decreased by the wave–mean–flow interaction. This requires initial small waves’ amplitudes to prevent a large reduction of the shear during the evolution of the system.

IV. RELATIONS WITH KURAMOTO-LIKE COUPLED OSCILLATORS

The phase-amplitude dynamics of equation set (1) resembles well-known models of phase interaction among two coupled oscillators [17–19] and is particularly similar to the phase dynamics of Stuart-Landau-type equations [1,13] in the limit of neutrally stable cycles [18]. The neutral stability of amplitudes is the main difference from commonly analyzed models of complex-amplitude equations and phase oscillators. While in those systems the Kuramoto dynamics is a result of a physically present balance of energy generation and dissipation (viscosity effects), both the HG model and the extended model considered here are assumed inviscid, and therefore they do not incorporate amplitude dissipation. Consequently, their states are fully determined by the initial conditions and by the conservations of wave action and pseudoenergy.

To further elaborate on relations to oscillators, we generalize equation set (1) to an ensemble of interacting vorticity waves by a discretization of the shear profile into N interfaces at positions y_j . Each of the interfaces then hosts a localized vorticity wave with amplitude $\mathcal{A}(y_j) = \mathcal{A}_j$ and phase $\epsilon(y_j) = \epsilon_j$ [20] that evolves according to

$$\dot{\mathcal{A}}_i = \sum_{j \neq i}^N \mathcal{A}_j \sigma_{i,j} \sin(\epsilon_i - \epsilon_j), \quad (22)$$

$$\dot{\epsilon}_i = -\omega_i(\mathcal{A}_i) + \sum_{j \neq i}^N \sigma_{i,j} \frac{\mathcal{A}_j}{\mathcal{A}_i} \sin(\epsilon_i - \epsilon_j + \delta), \quad (23)$$

where $\delta = \pi/2$. It becomes clear that the wave-wave–mean–flow interaction can be indeed regarded as a specific type of Kuramoto-Sakaguchi dynamics [21,22]. For such models, it is well known that there exist three main factors that influence the emergence of patterns of synchrony among oscillating units: (i) the form of the frequency distribution, (ii) the coupling topology, and (iii) the phase lag parameter δ in the phase interaction. The emerging patterns are a mixture of order (synchrony) and disorder (chaos/turbulence) [23–25] known as chimera states [26–29]. Thus, the N -interface-model, given by (23), is expected to accommodate chimera states, as it incorporates the following three ingredients:

(i) The distribution of natural wave frequencies is determined by the mean-flow profile [at least bimodal if $U(y) \sim \tanh(y)$]. Interestingly, the frequencies are also spatially correlated due to the spatial dependence of the mean flow as $\omega = kU(y) + kc(y)$.

(ii) The coupling strength of two wave interfaces i, j depends on the distance $y_i - y_j$ between them and is given by Green’s function $G(y_i - y_j)$, representing the evanescent structure of the far-field velocity, induced by the waves’ vorticity fields. For instance, in open boundaries, the simplest Green function decays exponentially with the distance between the interfaces, $G(y_i - y_j) \sim \exp(-k|y_i - y_j|)$ [20,30].

(iii) The appearance of a phase lag $\delta = \pi/2$ suggests a neutral coupling between repulsion and attraction of the waves.

Particularly interesting in the given N -interface model of shear waves is that each phase dynamics is coupled to the evolution of amplitudes such that the coupling coefficients (and the frequency of oscillations) are time-varying. Nevertheless, we see that Eq. (23) comprises Kuramoto solutions if all amplitudes are similar. Thus, low dimensional descriptions of the N -wave dynamics could exist. In fact, such descriptions have been exactly found for Kuramoto-like oscillators where they lead to a set of just three free variables, constrained by $N - 3$ constants of motion [9,31–35]. Nonetheless, the wave interaction model requires an extended analysis beyond the Kuramoto manifold [36] due to the presence of amplitude dynamics. Such an analysis was put forward earlier [37], but it is still not fully understood.

The N -wave interaction model can be understood as a second-order Kuramoto dynamics [38,39]. A reminiscence of this can be realized from a combination of phase and amplitude dynamics in Eqs. (11) or (12):

$$\frac{d^2 \epsilon}{d\tau^2} = 2(\gamma_0 \sin \epsilon - \sin 2\epsilon). \quad (24)$$

This equation describes the motion of a bead on a rotating hoop in the hypothetical situation where the centrifugal force is acting inwards [40]. Then γ_0 is equal to twice the ratio between the magnitude of the gravity and the centrifugal forces, whereas time is scaled by half of the frequency of the rotating hoop. Alternatively, Eqs. (11) or (12) can be written as a second-order amplitude equation:

$$\frac{d^2 \tilde{\mathcal{A}}}{d\tau^2} = 2\tilde{\mathcal{A}}[(\tilde{\mathcal{A}} - \tilde{\mathcal{A}}_0) + (2 - \mu_0)]. \quad (25)$$

V. DISCUSSION

Nonlinear shear instability is a highly complex mechanism [41], even when considering the high Reynolds number inviscid limit. Consequently, any minimal model that is focusing only on one, or several, aspects of the dynamics is somewhat naive and incomplete by construction. Yet, we find it instructive to isolate the different processes in order to deepen our physical understanding on this mechanism. For the linearized dynamics, the understanding of shear instability in terms of action at a distance interaction between counterpropagating vorticity waves has been found helpful, both conceptually and computationally. Here, we therefore looked for the next step to understand the basic interplay between waves, emerging from the linearized unstable normal modes, and the mean flow. While the model supports different regimes of dynamics, the main result of our analysis is quite straightforward—when the waves' amplitudes become large enough to interact with the mean flow, they “inviscidly” reduce their growth rate and start to librate around the neutral antiphased configuration with a mean finite amplitude.

How relevant is this mechanism to real hydrodynamical systems? For stratified shear flow, such as the Taylor-Caulfield setup of plane-Couette flow with two density interfaces, the unstable linearized dynamics is well described by the linearized model of Heifetz and Guha. There, the vorticity waves are the two counterpropagating interfacial gravity waves at the two interfaces [42]. The nonlinear evolution of the Taylor-Caulfield instability has been investigated in [43], and it is clear from their simulations (cf. their videos in the supplementary material) that as the waves reach finite amplitudes, they become unlocked from their unstable modal phase, and their phase difference increases toward π . However, the waves do not exhibit libration as resonant triad interaction ($k \iff 2k$) becomes the dominant mechanism. Indeed, in a follow-up study we intend to include resonant triad interactions [16,44] in the truncated form suggested by [45].

It is also interesting to compare our model with the evolution of finite amplitude Rossby waves in baroclinic shear instability. The latter is a central mechanism in geophysical fluid dynamics, where Rossby waves extract energy from the jet stream to form the weather systems in the midlatitudinal atmosphere [46]. The seminal weakly nonlinear analysis by Pedlosky [47] of the two-layer Phillips model [12] suggests libration around the zero phase between the waves rather than around π . The main reason for that is the relation between the baroclinic vertical shear with the mean potential vorticity (PV) gradients at the two layers (via the thermal wind balance), so that reduction in the mean shear reduces the mean PV gradients in the two layers and therefore it reduces the efficiency of the Rossby wave's intrinsic counterpropagation mechanism (represented by $c_{1,2}$ in our model) and their interaction coefficients (represented by $\sigma_{1,2}$ in our model). Consequently, when the mean shear is reduced by the Rossby wave PV flux, the counterpropagation speeds of the waves decrease as well, and it turns out that the latter effect overwhelms the former. This can be understood when writing our control parameter $\mu = \frac{k}{\sigma}[(|U_1| + |U_2|) - (|c_1| + |c_2|)]$. In our model, we assumed that only the mean flow is reduced when the

waves grow nonlinearly [that is, $(|U_1| + |U_2|)$ decreases and consequently μ decreases]. In the baroclinic model, however, $(|c_1| + |c_2|)$ decreases as well and even more intensively than the mean flow. This causes μ to grow rather than to decay as the waves grow and consequently the libration is reversed toward the zero phase. It is still interesting, however, how the nature of the libration (Fig. 5 in [47] and Fig. 7.16.6 in [12]) resembles the libration in Fig. 4. A crude but straightforward way to represent this process in the minimal model is to allow the wave–mean–flow interaction coefficients, $\beta_{1,2}$ in (5), to take negative sign.

Our minimal model is essentially 2D (streamwise and cross-stream). This does not pose a problem in the linearized stage of the instability, even when describing the canonical “2.5D” baroclinic setups [12]. However, as was shown by [47], in the weakly nonlinear regime one cannot ignore the generation of spanwise (meridional, in the baroclinic case) curvature of the jet, which in turn acts to reduce further the mean PV gradient in the lower layer by generating an effective “ β -plane stabilizing effect.” The spanwise dynamics in nonlinear shear instability is indeed robust to maintain the nonlinear generic self-sustaining process in shear flows, as explained by Waleffe [48]. It is therefore on our “to-do” list to extend our model to describe the essence of the Waleffe 3D wave–mean–flow interaction self-sustaining circle. The need for a three-dimensional minimal model is evident as well when considering baroclinic instability from the generalized Lagrangian mean (GLM) framework, where both the effect of the Stokes drift and the GLM meridional velocity should be taken into account [49]. A somewhat more straightforward for implementation, but still an important aspect of the nonlinear dynamics, is the role played by the critical layer in between the interacting waves. This phenomenon, for the linearized dynamics, considering a wave interaction minimal model has been addressed in [42]. We plan as well to include its interaction with the mean flow in a follow-up work.

In a different aspect, we find it interesting that the presented weakly nonlinear N -interfaces model, Eq. (23), relates to the well-studied Kuramoto-Sakaguchi dynamics. On the one hand, we identify all major ingredients for the emergence of chimera states. On the other hand, the existence of additional amplitude degrees of freedom is expected to result in additional challenges to understand the shear-wave dynamics from the perspective of coupled oscillators. Lastly, the concept of wave (entities) interacting in a distance, while altering their local mean flow (local surrounding), might be relevant to resemble some features of the dynamics of active matter [50]. Such an implementation, while intriguing, is less straightforward and requires more thinking.

ACKNOWLEDGMENTS

E.G. thanks the Joint Postdoctoral Fellowship Programme by Tel Aviv University and the University of Potsdam. E.H. is grateful to the Israeli Science Foundation (Grant No. 1645/19) and to the PAZY Foundation (Grant No. 324-2/22). Both authors thank Rok Cestnik, Oleh Omelchenko, and Anirban Guha for helpful discussion.

- [1] E. Heifetz and A. Guha, Normal form of synchronization and resonance between vorticity waves in shear flow instability, *Phys. Rev. E* **100**, 043105 (2019).
- [2] B. J. Hoskins, M. E. McIntyre, and A. W. Robertson, On the use and significance of isentropic potential vorticity maps, *Q. J. R. Meteorol. Soc.* **111**, 877 (1985).
- [3] N. Harnik, E. Heifetz, O. M. Umurhan, and F. Lott, A buoyancy-vorticity wave interaction approach to stratified shear flow, *J. Atmos. Sci.* **65**, 2615 (2008).
- [4] J. R. Carpenter, E. W. Tedford, E. Heifetz, and G. A. Lawrence, Instability in stratified shear flow: Review of a physical interpretation based on interacting waves, *Appl. Mech. Rev.* **64**, 060801 (2011).
- [5] E. Heifetz and A. Guha, A generalized action-angle representation of wave interaction in stratified shear flows, *J. Fluid Mech.* **834**, 220 (2018).
- [6] L. Biancofiore, F. Gallaire, and E. Heifetz, Interaction between counterpropagating Rossby waves and capillary waves in planar shear flows, *Phys. Fluids* **27**, 044104 (2015).
- [7] E. Heifetz, J. Mak, J. Nycander, and O. M. Umurhan, Interacting vorticity waves as an instability mechanism for magnetohydrodynamic shear instabilities, *J. Fluid Mech.* **767**, 199 (2015).
- [8] R. Yellin-Bergovoy, E. Heifetz, and O. M. Umurhan, Physical mechanism of centrifugal-gravity wave resonant instability in azimuthally symmetric swirling flows, *Phys. Rev. Fluids* **2**, 104801 (2017).
- [9] D. Witthaut and M. Timme, Kuramoto dynamics in Hamiltonian systems, *Phys. Rev. E* **90**, 032917 (2014).
- [10] E. Heifetz, C. Bishop, B. Hoskins, and J. Methven, The counter-propagating Rossby-wave perspective on baroclinic instability. I: Mathematical basis, *Q. J. R. Meteorol. Soc.* **130**, 211 (2004).
- [11] J. Methven, B. J. Hoskins, E. Heifetz, and C. H. Bishop, The counter-propagating rossby-wave perspective on baroclinic instability. Part IV: Nonlinear life cycles, *Q. J. R. Meteorol. Soc.* **131**, 1425 (2005).
- [12] J. Pedlosky *et al.*, *Geophysical Fluid Dynamics* (Springer, New York, NY, 1987), Vol. 710.
- [13] I. S. Aranson and L. Kramer, The world of the complex ginzburg-landau equation, *Rev. Mod. Phys.* **74**, 99 (2002).
- [14] S. Gupta, A. Campa, and S. Ruffo, Kuramoto model of synchronization: equilibrium and nonequilibrium aspects, *J. Stat. Mech.* (2014) R08001.
- [15] R. Salmon, Hamiltonian fluid mechanics, *Annu. Rev. Fluid Mech.* **20**, 225 (1988).
- [16] L. Biswas and P. Shukla, Resonant triad interactions in a stably stratified uniform shear flow, *Phys. Rev. Fluids* **7**, 023904 (2022).
- [17] B. Pietras and A. Daffertshofer, Network dynamics of coupled oscillators and phase reduction techniques, *Phys. Rep.* **819**, 1 (2019).
- [18] E. Gengel, E. Teichmann, M. Rosenblum, and A. Pikovsky, High-order phase reduction for coupled oscillators, *J. Phys. Complex.* **2**, 015005 (2021).
- [19] A. Pikovsky, M. Rosenblum, and J. Kurths, *A Universal Concept in Nonlinear Sciences* (Cambridge University Press, Cambridge, UK, 2001), Vol. 2.
- [20] E. Heifetz, N. Harnik, and T. Tamarin, Canonical hamiltonian representation of pseudoenergy in shear flows using counter-propagating rossby waves, *Q. J. R. Meteorol. Soc.* **135**, 2161 (2009).
- [21] O. E. Omel'chenko and M. Wolfrum, Bifurcations in the sakaguchi-kuramoto model, *Physica D* **263**, 74 (2013).
- [22] H. Sakaguchi and Y. Kuramoto, A soluble active rotator model showing phase transitions via mutual entertainment, *Prog. Theor. Phys.* **76**, 576 (1986).
- [23] C. C. Gong, C. Zheng, R. Toenjes, and A. Pikovsky, Repulsively coupled kuramoto-sakaguchi phase oscillators ensemble subject to common noise, *Chaos* **29**, 033127 (2019).
- [24] E. Teichmann and M. Rosenblum, Solitary states and partial synchrony in oscillatory ensembles with attractive and repulsive interactions, *Chaos* **29**, 093124 (2019).
- [25] S. W. Haugland, A. Tosolini, and K. Krischer, Between synchrony and turbulence: intricate hierarchies of coexistence patterns, *Nat. Commun.* **12**, 5634 (2021).
- [26] Y. Kuramoto and D. Battogtokh, Coexistence of coherence and incoherence in nonlocally coupled phase oscillators, [arXiv:cond-mat/0210694](https://arxiv.org/abs/cond-mat/0210694).
- [27] D. M. Abrams and S. H. Strogatz, Chimera States for Coupled Oscillators, *Phys. Rev. Lett.* **93**, 174102 (2004).
- [28] E. A. Martens, E. Barreto, S. H. Strogatz, E. Ott, P. So, and T. M. Antonsen, Exact results for the Kuramoto model with a bimodal frequency distribution, *Phys. Rev. E* **79**, 026204 (2009).
- [29] Z. G. Nicolaou, H. Riecke, and A. E. Motter, Chimera States in Continuous Media: Existence and Distinctness, *Phys. Rev. Lett.* **119**, 244101 (2017).
- [30] E. Heifetz and J. Methven, Relating optimal growth to counter-propagating rossby waves in shear instability, *Phys. Fluids* **17**, 064107 (2005).
- [31] S. Watanabe and S. H. Strogatz, Constants of motion for superconducting josephson arrays, *Physica D* **74**, 197 (1994).
- [32] M. Wolfrum, S. V. Gurevich, and O. E. Omel'chenko, Turbulence in the ott-antonsen equation for arrays of coupled phase oscillators, *Nonlinearity* **29**, 257 (2016).
- [33] M. S. Alber, G. G. Luther, J. E. Marsden, and J. M. Robbins, Geometric phases, reduction and lie-poisson structure for the resonant three-wave interaction, *Physica D* **123**, 271 (1998).
- [34] H. Nakao, Phase reduction approach to synchronisation of nonlinear oscillators, *Contemp. Phys.* **57**, 188 (2016).
- [35] E. Ott and T. M. Antonsen, Low dimensional behavior of large systems of globally coupled oscillators, *Chaos* **18**, 037113 (2008).
- [36] R. Cestnik and A. Pikovsky, Hierarchy of Exact Low-Dimensional Reductions for Populations of Coupled Oscillators, *Phys. Rev. Lett.* **128**, 054101 (2022).
- [37] S. Petkoski and A. Stefanovska, Kuramoto model with time-varying parameters, *Phys. Rev. E* **86**, 046212 (2012).
- [38] N. V. Barabash, V. N. Belykh, G. V. Osipov, and I. V. Belykh, Partial synchronization in the second-order kuramoto model: An auxiliary system method, *Chaos* **31**, 113113 (2021).
- [39] H. Taher, S. Olmi, and E. Schöll, Enhancing power grid synchronization and stability through time-delayed feedback control, *Phys. Rev. E* **100**, 062306 (2019).
- [40] S. H. Strogatz, *Nonlinear Dynamics and Chaos* (Westview, Philadelphia, PA, 2015).
- [41] X. Wu, Nonlinear theories for shear flow instabilities: physical insights and practical implications, *Annu. Rev. Fluid Mech.* **51**, 451 (2019).

- [42] A. Rabinovich, O. Umurhan, N. Harnik, F. Lott, and E. Heifetz, Vorticity inversion and action-at-a-distance instability in stably stratified shear flow, *J. Fluid Mech.* **670**, 301 (2011).
- [43] T. S. Eaves and C. P. Caulfield, Multiple instability of layered stratified plane couette flow, *J. Fluid Mech.* **813**, 250 (2017).
- [44] A. Guha and M. Rahmani, Predicting vortex merging and ensuing turbulence characteristics in shear layers from initial conditions, *J. Fluid Mech.* **878**, R4 (2019).
- [45] T. Tamarin, E. Heifetz, O. M. Umurhan, and R. Yellin, On the nonnormal-nonlinear interaction mechanism between counter-propagating rossby waves, *Theor. Comput. Fluid Dyn.* **29**, 205 (2015).
- [46] G. K. Vallis, *Atmospheric and Oceanic Fluid Dynamics: Fundamentals and Large-scale Circulation* (Cambridge University Press, Cambridge, UK, 2006).
- [47] J. Pedlosky, Finite-amplitude baroclinic waves, *J. Atmos. Sci.* **27**, 15 (1970).
- [48] F. Waleffe, On a self-sustaining process in shear flows, *Phys. Fluids* **9**, 883 (1997).
- [49] T. Shepherd, Mean motions induced by baroclinic instability in a jet, *Geophys. Astrophys. Fluid Dyn.* **27**, 35 (1983).
- [50] S. Motsch and E. Tadmor, A new model for self-organized dynamics and its flocking behavior, *J. Stat. Phys.* **144**, 923 (2011).